Origin of a Nanoindentation Pop-in Event in Silicon Crystal

R. Abram, D. Chrobak, and R. Nowak

Phys. Rev. Lett. **118**, 095502 — Published 3 March 2017

DOI: 10.1103/PhysRevLett.118.095502

The Origin of Nanoindentation Pop-in Event in Silicon Crystal

R. Abram[1], D. Chrobak[1,2], and R. Nowak[1,3*]

[1] *Nordic Hysitron Laboratory, Department of Chemistry & Materials Science, School of Chemical Engineering, Aalto University, 00076 Aalto, Finland*

[2] *Institute of Materials Science, University of Silesia, 75 Pułku Piechoty 1 A, 41-500 Katowice-Chorzów, Poland*

[3] *Extreme Energy-Density Research Institute, Nagaoka University of Technology, 1603-1 Kami-Tomioka-Chou, Nagaoka, Niigata 940-2188, Japan*

The Letter concerns surface nanodeformation of Si-crystal using atomistic simulation. Our results account for both the occurrence and absence of pop-in events during nanoindentation. We have identified two distinct processes responsible for indentation deformation based on load-depth response, stress-induced evolution of crystalline structure and surface profile. The first, resulting in a pop-in, consists in the extrusion of the crystalline high pressure Si-III/XII phase, while the second, without a pop-in, rely on a flow of amorphized Si to the crystal surface. Of particular interest to silicon technology will be our clarification of the interplay among amorphization, crystal-to-crystal transition and extrusion of transformed material to the surface.

*Email: Roman.Nowak@aalto.fi

PACS numbers: 02.70.Ns, 62.20.-x, 61.50.-f, 64.70.K-, 64.70.kg, 64.70.Nd

Increasing accuracy of nanoindentation experiments has resulted in the detection of pop-in discontinuities in the load-depth *P-h* curves [1], which reflect sudden progress in the deformation of a highly stressed nanovolume located under the tip. The phenomenon observed for numerous metallic crystals [2-4], GaN [5], SiC [6], Si-nanoobjects [7-9], is linked to nucleation of dislocations in the virtually defect-free crystal nano-volume stressed under an indenter. The first pop-in in the *P-h* graph usually defines incipient plasticity of the probed material, which relates to either dislocation nucleation [2-9] or pressure-induced phase transformation, such as in the case of GaAs [9,11]. However, the pop-ins recorded for silicon seem different, since their number and location are neither predictable nor repeatable [12-14]. Numerous reports on nanoindentation in silicon provide examples of the *P-h* curves displaying either single, double, triple discontinuities, or none at all (Fig. S1 in Ref. 15). The majority of experiments proceed along a pop-in free loading path [15], while the detected discontinuities tend to be assigned either to the formation of slip bands and cracks [12,16], or to pressure-induced phase transformations in Si (*e.g.,* [17-19]). This widely accepted scenario was altered by Bradby *et al.* [13], who linked the pop-in event to extrusion, *i.e.,* the transportation of a high-pressure Si-II phase (β-Sn structure) beyond the stressed region, and its subsequent amorphization at the surface.

Our analysis of the Si pop-in phenomenon reported in this Letter, takes in the abundant experimental data available [15] together with our molecular dynamics (MD) simulations. An inspection of the structural correlation functions, atoms' coordination numbers and their positions enabled us to clarify the role of high-pressure phases in the deformation of the Si crystal and to identify two principal mechanisms which account for its indentation behavior. The first, responsible for the pop-in event, concerns the extrusion of the crystalline Si-III/XII phase nanovolume and its subsequent amorphization at the surface. In contrast, the second - which involves material that has undergone pressure-induced amorphization, flowing steadily from beneath the acting indenter to the surface - does not result in pop-ins of any kind in the indentation load-depth *P-h* curve. This resolves the long-standing paradox [15] of Si-crystal indentation whereby pop-ins are by turns experimentally attested and disproven.

Our MD simulations performed with the LAMMPS code [20], concerned indentation of Si-cluster (size of 43.448 × 43.448 × 21.724 nm) with the perfect diamond structure (a =5.431 Å) composed of 2060800 atoms. The interactions among Si atoms were defined by the three-body Tersoff-type interatomic potential [21] capable of capturing phase transformations between crystalline silicon structures [19,22-24,26-28]. The interaction between the Si-crystal and a rigid, diamond, cono-spherical tip (the half apex angle of π/4, radius of R=5 nm) was defined by the repulsive Morse potential (cutoff radius 3 Å). The system was initially relaxed to zero-force configuration using the conjugate gradient method, while the employment of Nosé-Hoover canonical thermostat for 1 ns, enabled the equilibration of the system at 230 K. The procedure repeated during simulations with the displacement-increment of 0.5 Å and relaxation time of 20 ps represents depth-controlled indentation.

The total potential energy E_{pot} of the crystal-tip system was averaged over 50 time-increments, at the end of 20 ps long relaxation at each stage of penetration. As a result, the relationship $P= \square\ dE_{pot}/dh$ [10] enabled us to determine the P-h curve with pop-ins initiated at indentation depths of $h_A \approx 9$ and $h_B \approx 10$ nm (Fig. 1). The observed A and B load-declines mark pop-in events registered in depth-controlled experiments [3,9], similarly to the multiple pop-in phenomenon reported in early silicon research [12,15,25].

The calculated depth-profile of contact stress p_c-h (Ref. 29 and Fig. 1b), provides the characteristic 12.4 and 12.1 GPa values that mark the onset of the A and B pop-ins, while the Si-I→Si-II transformation was found to occur when the mean value of p_c reaches its maximum of $\langle p_c \rangle_{max} \approx 13.5$ GPa ($h \approx 1$ nm). The absence of pop-ins close to the $\langle p_c \rangle_{max}$-point touches on the familiar conundrum of 'the pop-in-free Si loading path' (Fig. S1b in Ref. 15), concurring with a number of previous findings, *e.g.,* [14], while remains at odds with others, *e.g.*, [12,18]. A subsequent rise of indentation depth causes the $\langle p_c \rangle$ to steadily decrease from 13.5 to 10.9 GPa, marking the interval ($1<h<11.5$ nm) at which silicon undergoes phase transitions (Fig. 1b).

We contend that the crystallographic similarity of Si-I and Si-II structures makes the Si pop-in virtually undetectable. Indeed, one can fit the Si-I cubic diamond (*cd*) unit cell with Si atoms in positions:

(0,0,0), (0.5,0.5,0.5), (0.5,0.0,0.25) and (0.0,0.5,0.75) into the tetragonal box (a_I=3.840 Å, c_I=5.431 Å). Thus the Si-I→Si-II transition would be regarded as a continuous change of *a* and *c* lattice constants until they reach the values a_{II}=4.665 Å. c_{II}=2.565 Å reported for Si-II at 11.7 GPa [28]. The relative atomic coordinates do not change along the indicated transition path.

The identification of high-pressure Si phases formed during the MD-simulated indentation was based on the available structural data [23,24,26-28] and the Si atoms' coordination number (nearest neighbors, *NN*). As a result - in addition to the Si-I and Si-II phases - we detected the following features of a highly stressed Si-crystal: (1) the BCT5-structure (body-centered tetragonal) with 5 nearest neighbors (*NN*=5; one at a distance of 2.31 Å and four at 2.44 Å); (2) the Si-III phase (bc8, body-centered-cubic) represented by 4 nearest neighbors (*NN*=4) at 2.37 Å and a single non-bonded atom at distance of 3.41 Å (at 2 GPa); (3) the Si-XII structure (r8, rhombohedral) with 4 nearest neighbors (*NN*=4) at a distance of 2.39 Å and a non-bonded one at 3.23 or 3.36 Å (at 2 GPa); as well as (4) the amorphized Si. Following a common procedure, the location of the fifth non-bonded atom, at the distance of 2.6 to 3.5 Å, was used to distinguish the four-coordinated Si-I structure from Si-III and Si-XII ones.

The stressed Si structure (Fig. 2) displays a large amorphous zone (mixture of red and yellow atoms) with a minute seed of crystalline Si-II phase (yellow nano-volume, *NN*=6), formed right under the tip. The indicated area is surrounded by the high-pressure crystalline BCT5-phase (red atoms, *NN*=5), while the entire zone is immersed in a mixture of metastable structures Si-III/XII (black atoms, *NN*=4) residing at a certain distance from the tip. The exception is the B'-location, where Si-III, Si-XII and BCT5 phases emerge. The straight lines resembling slip-bands and composed of otherwise coordinated atoms (Si-II, *NN*=6) confirm the crystalline character of the phases in B' location, close to the Si-crystal surface. Consequently, we obtained the complete scenario of structural changes induced in Si crystal directly under the diamond tip (Fig. 2), which agrees with previous achievements [22-24,26-28,30-32] and vindicates our MD-procedure with the Tersoff-type potential.

Since it is hard to expect the Si-II nano-volume to be transported to the distant surface (see Fig. 2), our findings call into question the widely accepted perception of the pop-in as linked to the extrusion of

the Si-II phase and its subsequent amorphization [13]. The determined number *N(h)* of Si atoms displaced during indentation above the original surface-level point to four distinct areas: A_1', A_2', α' and B', where extrusion is initiated sequentially at *h* of 9.0, 9.2, 9.3, and 9.9 nm (Fig. 3a). A detailed inspection of the *P-h* data (Fig. 3b) revealed the pop-in A composed of the pair of displacements (A_1-A_2) and the next pop-in B, while the extrusion of an amorphous Si starts at α-point. The extrusions in A_1', A_2', and α' regions contribute to the pop-in A (Fig. 1a), while extrusion in the B' area is responsible for the pop-in B (see the points' order A_1, A_2, α and B in Fig. 3b).

Interestingly, the A and B pop-ins appear linked to the transport of a crystalline nano-volume to the surface, while extrusion of the amorphous α-Si does not leave any detectable trace in the *P-h* curve (Fig. 3b). This calls for the establishment of a pop-in related extrusion criterion. A comparison of the potential energy E_{pot} (defined as the sum of energy interaction among all the atoms within a relevant zone) calculated for the A_1' (Fig. 3c) and α' (Fig. 3d) areas confirms a striking difference between the two cases. While the former plot displays the characteristic perturbation which derivative reveals the A_1 pop-in (Fig. 3b), the latter exhibits a relationship which does not result in any pop-in. These results led us to conclusion that the indentation deformation of silicon, although based solely on the extrusion of stressed material – as advocated by Bradby *et al*. [13] and Gerbig *et al*. [14,33] – is governed by two essentially different mechanisms M1 and M2.

The sequence *i-iv* of snapshots (Fig. 4a and the animation 'Mech-1' [15]), illustrates the consecutive stages of structure evolution at the depth of 8.2, 8.7, 9.5 and 11.2 nm, which defines the mechanism M1. As the penetration proceeds, the minute volumes (left and right) of the crystalline Si-III/XII structure, surrounded by the BCT5-phase, develop in both A_1' and A_2' locations (Fig. 4a-*iii*). The formation of the crystalline Si-III/XII 'nano-grains' does not proceed symmetrically (Fig. 4a-*ii*), which explains the double pop-in A_1-A_2 pattern (Fig. 3b). The MD-simulations reveal a sudden extrusion of the entire Si-III/XII crystallite when the pop-in appears (Fig. 3b and Fig. 4a-*iii-iv*). The transportation of the material results in stress relaxation reflected by the pop-in. At the surface, in the absence of high pressure, the extruded Si-

III/XII crystallite transforms into an amorphous Si (confirmed by bond angle distribution in Fig. S3 in Ref. 15). The M1-mechanism acts also in the B' area resulting in the appearance of the B pop-in (Fig. 3b and Fig. 4b). Thus, the M1-mechanism is similar to that described by Bradby *et al.* [13], however instead of Si-II phase, the other high-pressure structures (BCT5 and Si-III/XII) are extruded.

Although it is the M1-mechanism which produces pop-ins, the deformation of silicon is also significantly contributed by M2-mechanism - an extrusion of an amorphized Si (Fig. 4b and the animation 'Mech-2' in Ref. 15). The sequence of *v-viii* snapshots – illustrates the process, advancing in the α' region whose continuous character (Fig. 3d) precludes any prospect of a pop-in. Given the role amorphization plays in the nanoindentation of Si, the extrusion of α-Si offers an alternative explanation of the puzzle related to the frequent absence of pop-ins in the *P-h* curves. While our MD-simulations involved cono-spherical indentation, the lion part of experiments employ pyramidal tips [15], which facilitate amorphization due to their sharpness and excessive stress-concentration near the edges. It is quite possible that the indentation deformation is dominated in such cases by the M2-mechanism, leading to frequently reported pop-in free loading path, *e.g.*, [12,33,34].

Conclusions. - This Letter presents two distinct mechanisms responsible for the nanoindentation deformation of silicon *via* the extrusion to the surface of high-pressure phases formed beneath the acting tip. Our MD-simulations demonstrated the extrusion of a crystalline Si-III/XII phase nanovolume leading to a pop-in event, in contrast to the transportation of an amorphized Si to the surface, which produced no detectable discontinuity in the indentation *P-h* curve. Notably, the obtained results do not contradict the original findings by Minor and coworkers [7,8] concerning the *in situ* observation (indentation inside a TEM column) of the generated high-pressure Si phases and amorphization in Si nanowedges. The research advances our understanding of Si behavior, such as elastic-plastic transition and amorphization, which are of great interest to silicon science and technology [35], and could lead to new applications. It is also in line with the recent studies of crystalline-to-amorphous transition in silicon which attracts considerable attention [36,37].

Acknowledgements – The authors gratefully acknowledge A.M. Minor, who offered helpful comments on the initial version of the manuscript. We thank the Academy of Finland for its support under the OMA Research Program: the project 'PROPER' as well as the CSC-IT Center for Science for Computation Resources, Finland. DC acknowledges also funding from the National Science Center of Poland: grant DEC-2012/05/B/ST-8/02945. Last not least, our thanks are due to Hysitron Inc. (Minneapolis, USA) for long-standing support and access to their equipment and scientific database.

References

1. S.G. Corcoran, R.J. Colton, E.T Lilleodden, and W.W. Gerberich, Phys. Rev. B **55**, R16057 (1997).
2. C. A. Schuh, J. K. Mason, and A. C. Lund, Nature Materials **4**, 617 (2005).
3. J. K. Mason, A. C. Lund, and C. A. Schuh, Phys. Rev. B **73**, 054102 (2006).
4. J. Li, K. J. Van Vliet, T. Zhu, S. Yip, and S. Suresh, Nature **418**, 307 (2002).
5. M. Fujikane, T. Yokogawa, S. Nagao, and R. Nowak, Phys. Status Solidi C **8**, 429 (2011).
6. I. Szlufarska, A. Nakano, and P. Vashishta, Science **309**, 911 (2005).
7. A.M. Minor, E.T. Lilleodden, M. Jin, E.A. Stach, D. Chrzan, and J.W. Morris, Philos. Mag. **85**, 323 (2005).
8. D. Ge, A.M. Minor, E.A. Stach, and J.W. Morris, Philos. Mag. **86**, 4069 (2006).
9. D. Chrobak, N. Tymiak, A. Beaber, O. Ugurlu, W. W. Gerberich, and R. Nowak, Nature Nanotechnology **6**, 480 (2011).
10. D. Chrobak, K. Nordlund, and R. Nowak, Phys. Rev. Lett. **98**, 045502 (2007).
11. R. Nowak, D. Chrobak, S. Nagao, D. Vodnick, M. Berg, A. Tukiainen, and M. Pessa, Nature Nanotechnology **4**, 287 (2009).
12. T. Juliano, V. Domnich, and Y. Gogotsi, J. Mater. Res. **19**, 3099 (2004).
13. J. E. Bradby, J. S. Williams, and M. V. Swain, Phys. Rev. B **67**, 085205 (2003).
14. Y. B. Gerbig, S.J. Stranick, D. J. Morris, M. D. Vaudin, and R. F. Cook, J. Mater. Res. **24**, 1172 (2009).
15. See Supplemental Material at http://link.aps.org/supplemental/???/PhysRevLett.??? which contains - our statistics concerning pop-ins in Si-crystals (Fig. S1, S2 and Table S1), visualization of the structure evolution during indentations (movie 1 and 2), remarks about Si amorphization, inspection of structural correlation functions.
16. J. Bradby, J. Williams, J. Wong-Leung, M. Swain, and P. Munroe, J. Mater. Res. **16**, 1500 (2001).
17. S. Wong, B. Haberl, J. S. Williams, and J. E. Bradby, Appl. Phys. Lett. **106**, 252103 (2015).
18. L. Chang and L. Zhang, Mater. Sci. Eng. A **506**, 125 (2009).
19. Z. Zhang, A. Stukowski, and H. M. Urbassek, Comp. Mater. Sci. **119**, 82 (2016).

20. S. Plimpton, J. Comp. Phys. **117**, 1 (1995); URL: lammps.sandia.gov.
21. J. Tersoff, Phys. Rev. B **39**, 5566 (1989).
22. W. C. D. Cheong and L. C. Zhang, Nanotechnol. **11**, 173 (2000).
23. D. E. Kim and S. I. Oh, J. Appl. Phys. **104**, 013502 (2008).
24. Y. H. Lin, S. R. Jian, Y.-S. Lai, and P. F. Yang, Nanoscale Res. Lett. **3**, 71 (2008).
25. C. R. Das et al. Appl. Phys. Lett. **96**, 253113 (2010).
26. J. Sun, L. Fang, J. Han, Y. Han, H. Chen, and K. Sun, Comp. Mater. Sci. **82**, 140 (2014).
27. X. Du, H. Zhao, L. Zhang, Y. Yang, H. Xu, H. Fu, and L. Li, Sci. Rep. **5**, 16275 (2015).
28. J. Sun, A. Ma, J. Jiang, J. Han, and Y. Han, J. Appl. Phys. **119**, 095904 (2016).
29. The contact pressure was defined as $p_c=P/A$, where P is the applied load and $A=\pi R^2$ stands for contact area with the R-radius. Specifically, at the moment of pop-in events A and B the contact radii reach R_A=11.1 nm and R_B=12.1 nm, respectively.
30. G. S. Smith, E. B. Tadmor, and E. Kaxiras, Phys. Rev. Lett. **84**, 1260 (2000).
31. G. S. Smith, E. B. Tadmor, N. Bernstein, and E. Kaxiras, Acta mater. **49**, 4089 (2001).
32. A. Gannepalli and S. K. Mallapragada, Nanotechnol. **12**, 250 (2001).
33. Y. B. Gerbig, C. A. Michaels, A. M. Forster, and R. F. Cook, Phys. Rev. B **85**, 104102 (2012).
34. S. Wong, B. Haberl, J. S. Williams, and J. E. Bradby, J. Appl. Phys. **118**, 245904 (2015).
35. H. G. Craighead, Science **290**, 1532 (2000).
36. Y-C. Wang, W. Zhang, L-Y. Wang, Z. Zhuang, E. Ma, J. Li, and Z-W. Shan, NPG Asia Materials **8**, e291 (2016).
37. Y. He, L. Zhong, F. Fan, C. Wang, T. Zhu and S.X. Mao, Nature Nanotechnology **11**, 866 (2016).

Figures and captions

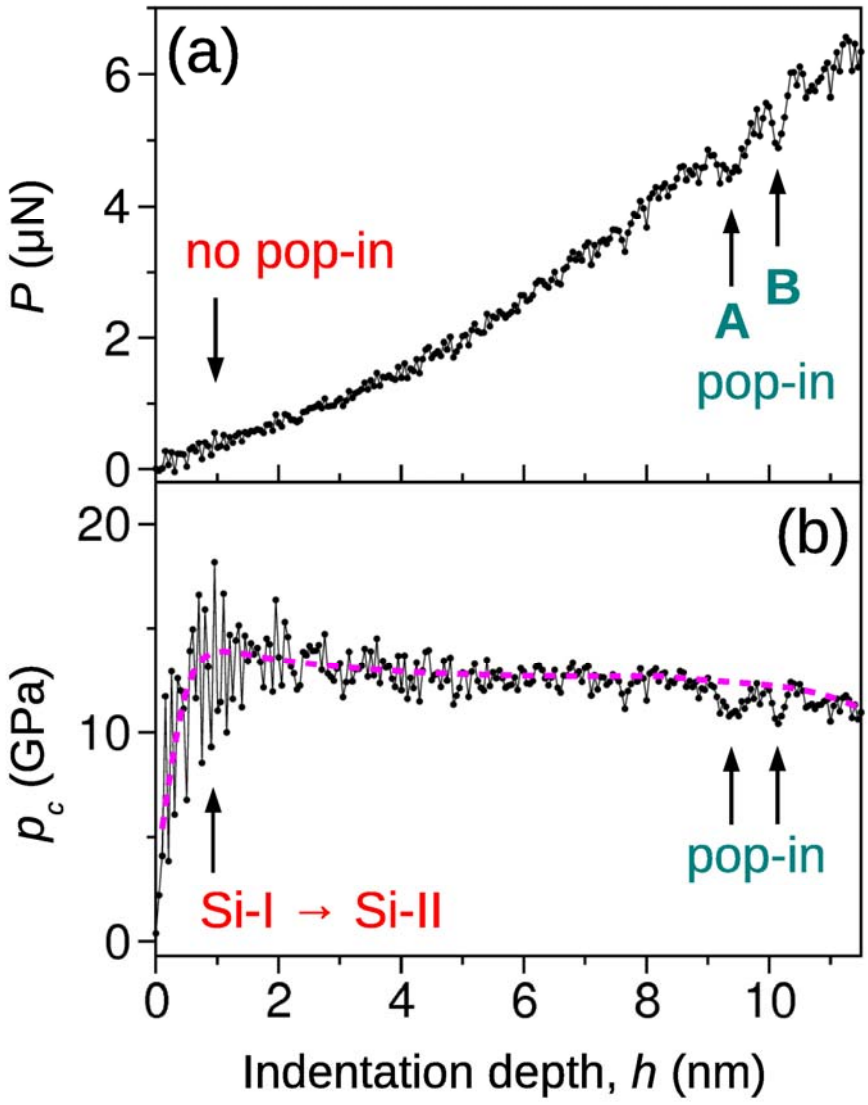

FIG. 1 (color). The history of the Si crystal nanodeformation reflected by the load-depth *P*-*h* curve (a) derived from MD-simulations and the contact pressure-depth p_c-*h* graph (b) that exposes the starting point of the Si-I→Si-II transformation. The latter occurs at early stage of nanoindentation (b) without any pop-in (a). The discontinuities (A and B) show up in the *P*-*h* curve as the indentation process progress.

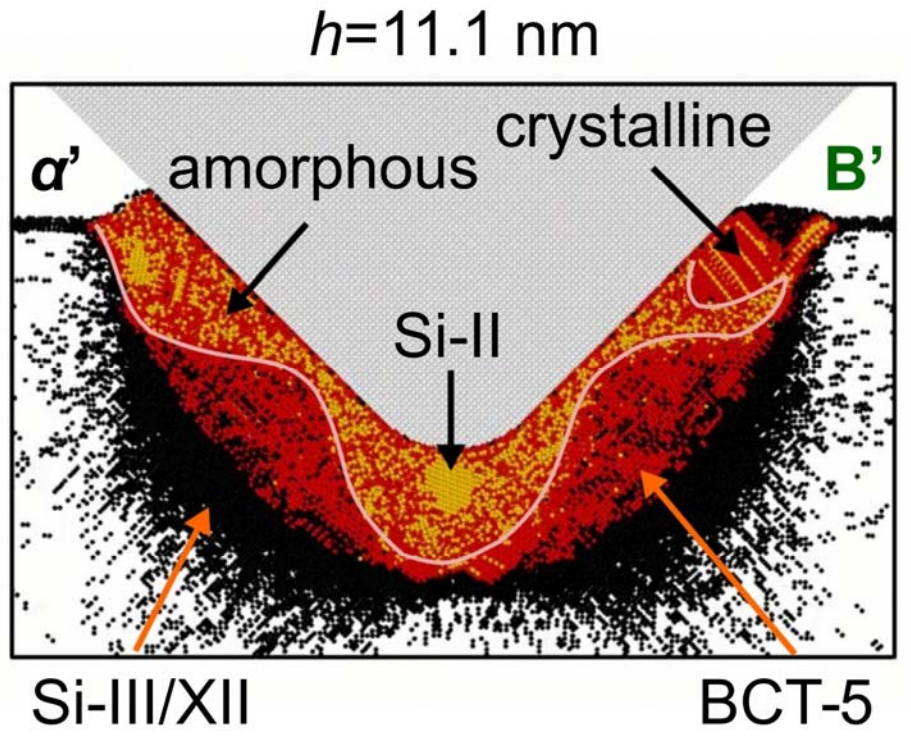

FIG. 2 (color). Identification of high-pressure phases formed during nanoindentation in Si crystal. The color of an atom denotes the *NN* number of its nearest neighbors (black-4, red-5 and yellow-6) and allows us to distinguish between the high-pressure formed crystallites of the BCT5 (*NN*=5), Si-II (*NN*=6) and metastable Si-III/XII (*NN*=4) phases [23,24,26-28]. The area from the indenter profile to pink border-line defines the location of pressure-amorphized silicon. The atoms of the initial Si-I phase are not displayed for clarity.

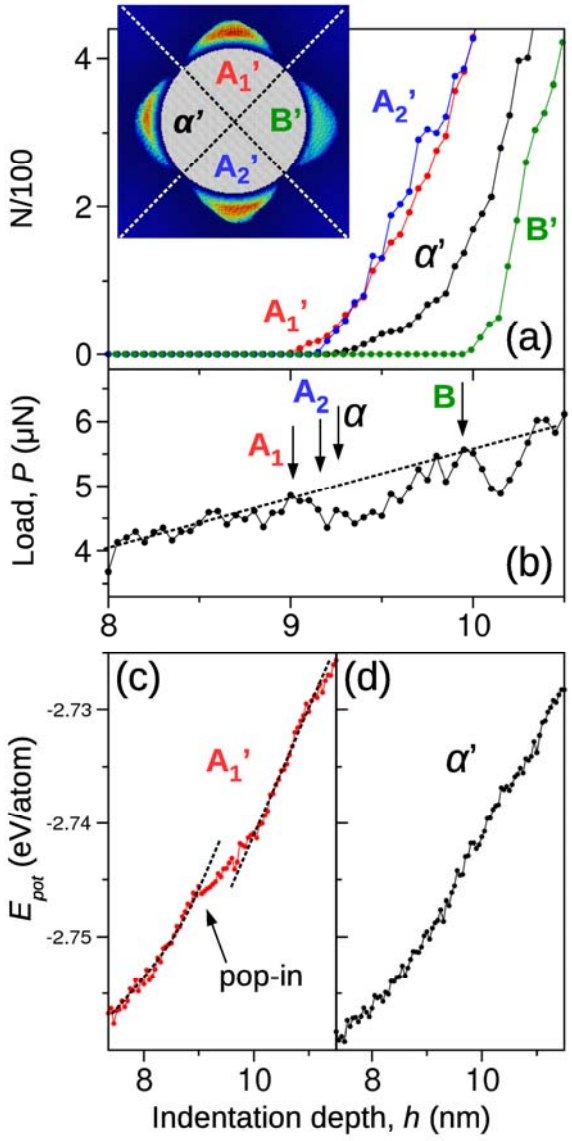

FIG. 3 (color). The results of MD-simulated indentation that enable us to define the pop-in events in the *P-h* curve and distinguish them from non-pop-in effects. The number *N* of Si atoms displaced above the crystal surface defines sequence of extrusion in the A_1', A_2', α' and B' zones. The zoomed *P-h* graph engulfs the A_1, A_2 and B pop-ins and exposes extrusion of amorphized Si at α-point (b). The indicated events are linked to the transport of deformed Si that occurs in the specific areas A_1', A_2', B' and α'. The striking discrepancy in $E_{pot}(h)$ profiles (discontinuity against smooth growth) recorded for A_1' (c) and α' (d) regions serves the criterion of pop-in detection in silicon.

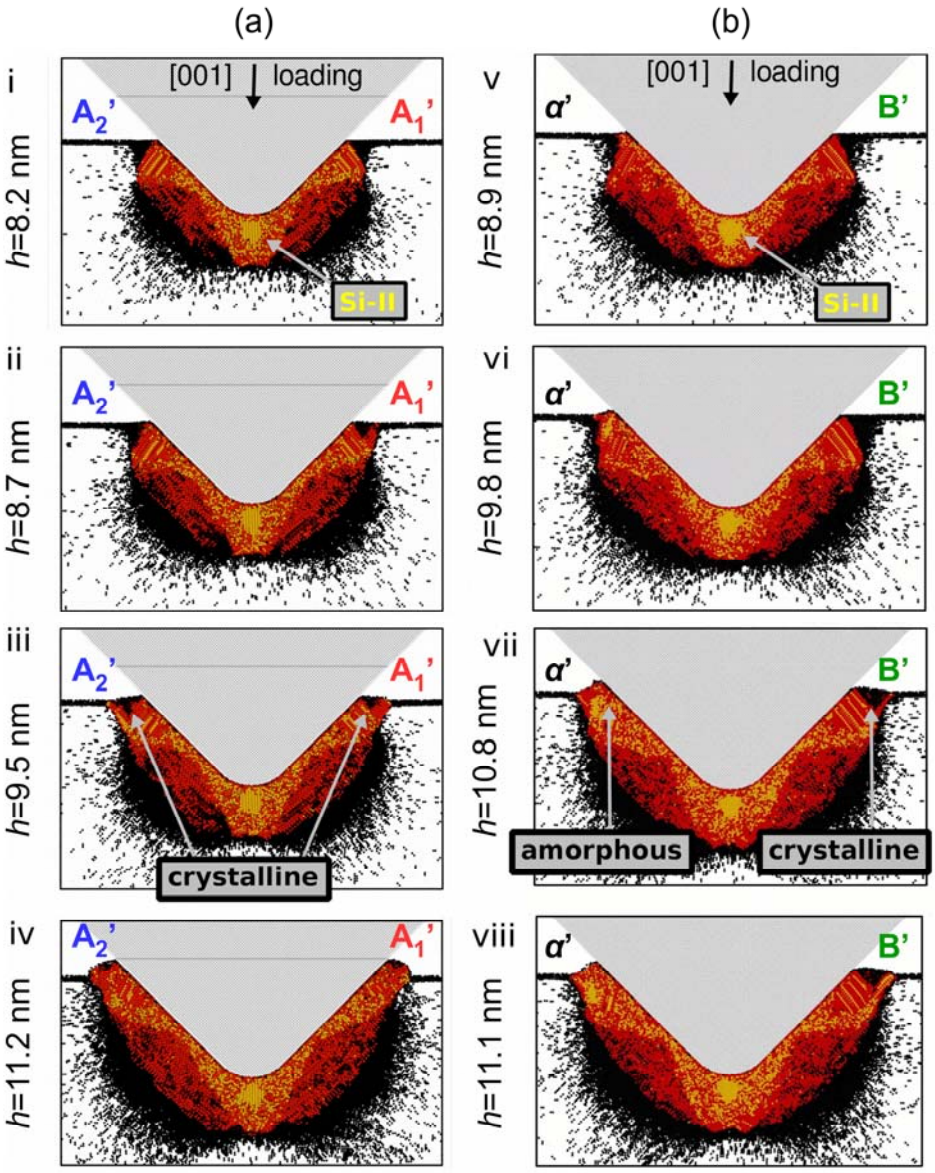

FIG. 4 (color). Structural changes during nanoindentation viewed along the direction perpendicular to the indentation axis (on the A_2'-A_1' and α'-B' cross-sections) that display the M1 (a) and M2 (b) mechanisms. The *i-iv* snapshots (a) illustrate the extrusion of a mixture of Si-III/XII phases in the A_1' and A_2' locations. The extrusion of minute crystallites in the A_1'-area is responsible for the formation of the pop-in A_1 – the 'M1 mechanism'. The α'- B' cross-section (b) reveals the amorphous Si in the α'-area (Fig. 3a) transported to the surface in accordance with Bradby *et al.* [13] (*v-viii* snapshots), and outlines the 'M2 mechanism' that causes no pop-in. The extrusion of the crystallite in the B-area (*v-viii* snapshots) results in the pop-in B (see Fig. 2).